Journal of Magnetic Resonance 328 (2021) 106993

Contents lists available at ScienceDirect

Journal of Magnetic Resonance

journal homepage: www.elsevier.com/locate/jmr

Optimal control pulses for subspectral editing in low field NMR

A. Bahti [a,b,*], A. Telfah [a], J. Lambert [a], R. Hergenröder [a,*], D. Suter [b]

[a] Leibniz-Institut für Analytische Wissenschaften - ISAS - e.V., 44139 Dortmund, Germany
[b] Experimental Physics III, TU Dortmund University, 44227 Dortmund, Germany

ARTICLE INFO

Article history:
Received 13 November 2020
Revised 14 March 2021
Accepted 26 April 2021
Available online 30 April 2021

Keywords:
Optimal control pulses
Krotov algorithm
Low field NMR
Spin system editing
Subspectral editing
Metabolite

ABSTRACT

Low field NMR is an inexpensive and low footprint technique to obtain physical, chemical, electronic and structural information on small molecules, but suffers from poor spectral dispersion, especially when applied to the analysis of mixtures. Subspectral editing employing optimal control pulses is a suitable approach to cope with the severe signal superpositions in complex mixture spectra at low field. In this contribution, the use of optimal control pulses is demonstrated to be feasible at a field strength as low as 0.5 T. The optimal control pulse shapes were calculated using the Krotov algorithm. Downsizing the complexity of the algorithm from exponential to polynomial is shown to be possible by using a system approach with each system corresponding to a (small) molecule. In this way compound selective excitation pulses can be calculated. The signals of substructures of the cyclopentenone molecule were excited using optimal control pulses calculated by the Krotov algorithm demonstrating the feasibility of subspectral editing. Likewise, for a mixture of benzoic acid and alanine, editing of the signals of either benzoic acid or alanine employing optimal control pulses was shown to be possible. The obtained results are very promising and can be extended to the targeted analysis of complex mixtures such as biofluids or metabolic samples at low field strengths opening access for benchtop NMR to point of care settings.
© 2021 Elsevier Inc. All rights reserved.

1. Introduction

Low field NMR spectroscopy [1–5] is a portable and inexpensive spectroscopic technique used to obtain physical, chemical, electronic and structural information about small molecules [6–11], as well as large systems such as lipids [12], polymers [12] and even rigid solids [13]. However, in the case of complex mixtures of compounds such as metabolomics samples, the limited spectral dispersion of low field NMR results in severe signal superpositions, that render the identification and quantification of individual compounds and crystals difficult.

In order to disentangle such complex superposition patterns, techniques like pure shift NMR [14] and diffusion ordered spectroscopy [15] have been successfully applied at low field strengths. Nevertheless, these approaches suffer from either poor sensitivity (pure shift NMR) or require pulsed field gradient equipment (DOSY), which may not be available. We here suggest an alternative approach based on subspectral editing to cope with the limitations and severe signal superpositions in complex mixture spectra at low field. Our approach is based on optimal control theory [16–18] which offers a convenient way to design selective radio-frequency pulses for a broad range of transformations. Possible transformations comprise spin-system selective pulses, that can be applied to set up subspectral editing experiments [19,20]. For the calculation of optimal control pulses, numerical simulation and optimization tools are indispensable. We used the Krotov algorithm [17,18] because it avoids convergence to local extremum points [17] and enhances the objective functional monotonically at each iteration [18]. Moreover, the algorithm is well suited for large spin systems [18] and can be used for broadband optimization problems with a large number of spin system parameters. In this respect, subspectral editing using optimal control pulses obtained with the Krotov algorithm is shown to be feasible at a field strength as low as 0.5 T. In addition, we demonstrate an approach to downsize the complexity of the algorithm, allowing targeted analysis of complex mixtures (Fig. 1).

2. Theory

In the context of optimal control theory, we focus on systems, the evolution of which is governed by a Hamiltonian dependent on external control fields. The dependence of the Hamiltonian on the control can be complicated, but often it suffices to consider a simple form such as a linear perturbation of the Hamiltonian

* Corresponding authors at: Leibniz-Institut für Analytische Wissenschaften - ISAS - e.V., 44139 Dortmund, Germany.
E-mail addresses: ahmed.bahti@isas.de (A. Bahti), roland.hergenroeder@isas.de (R. Hergenröder).

https://doi.org/10.1016/j.jmr.2021.106993
1090-7807/© 2021 Elsevier Inc. All rights reserved.

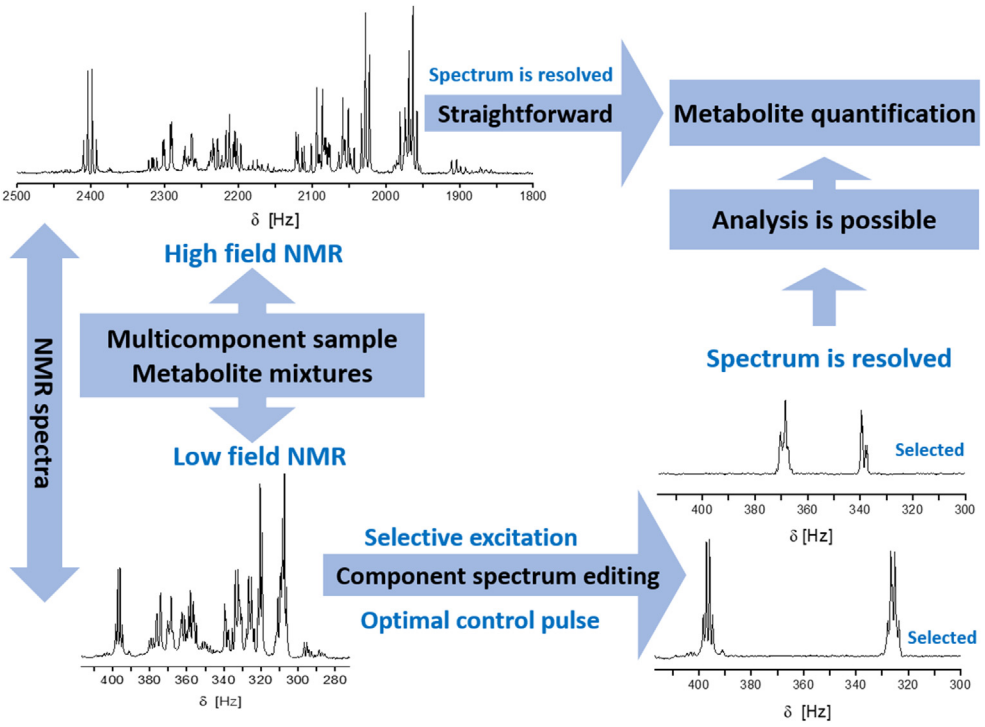

Fig. 1. Schematic description of the planned metabolite-specific spectral editing employing low field NMR.

$$H(t) = H_0 + \sum_k \omega_k I_k, \tag{1}$$

where H_0 and $\sum_k \omega_k I_k$ denote the system Hamiltonian and the control Hamiltonian, respectively. The control is designed to steer the system from an initial state to a target state. This optimization problem cannot be solved directly by analytical means and generally involves iterative algorithms, one of which is the Krotov algorithm [17,18]. It is based on the maximization of a functional J, given by

$$J = \varnothing - \lambda \int_0^T \sum_k \omega_k^2(t) dt \tag{2}$$

The maximization is actually performed by minimization of $-J$ [17], where λ denotes a penalty factor, T is the total duration of the pulse and $\varnothing$ is the quality factor. For the optimization of a propagator $U_{D,}$ the quality factor is given by

$$\phi = |\mathrm{Tr}\left(U^{'}{}_D U\right)|^2 \tag{3}$$

In order to take static and r.f. field inhomogeneity into account and to calculate a robust Krotov pulse, the quality factor term $\varnothing$ of the optimal control functional can be replaced by a sum $\sum_i \phi_i$ over a range of conditions

$$J = \sum_i |\mathrm{Tr}(U_D^{'} U_i)|^2 - \lambda \int_0^T \sum_k \omega_k^2(t) dt \tag{4}$$

where U_D is the desired propagator, U$^{'}$ being the adjoint of U and the U_i are the propagators corresponding to Hamiltonians (H_i) which characterize the transformation properties of the robust pulse. The H_i are derived as follows: The static field inhomogeneity (SFI) is taken into account by the introduction of additional resonance frequency terms with higher and/or lower resonance frequencies in the system's Hamiltonian, while the control Hamiltonian is left unchanged. On the other hand, in order to take into account radio-frequency field inhomogeneity (RFI), prefactors for the control amplitudes are introduced, while the system Hamiltonians are left unchanged. The Hamiltonians (H_i) are then used for the forward propagation of the U_i and the backward propagation of the B_i in every step of the iteration.

In order to reduce the exponential complexity of the algorithm, which poses a heavy computational burden on calculations of pulses for more than 8 spins, a system approach was introduced. The spin system of each chemical compound (I) is considered a system with a distinct system Hamiltonian $(H_{0,I})$, a distinct propagator $(U_{D,I})$ to be synthesized and a set of SFI/RFI propagators $(U_{i,I})$. The sums over all SFI/RFI conditions then reads

$$J = \sum_l \sum_i |Tr(U_{D,I}^{'} U_{i,l})|^2 - \lambda \int_0^T \sum_k \omega_k^2(t) dt \tag{5}$$

where l starts from 1 to number of SFI/RFI conditions,i starts from 1 to number of compounds in the sample and k starts from 1 to number of systems.

Further details about the algorithm can be found in the appendix.

3. Experimental details

We equipped the low field NMR system with a permanent homebuilt multilayer Halbach magnet with 0.486 T field strength, resulting in an operating frequency of 21.25 MHz for protons. The Halbach magnet has a B_0 homogeneity of $\frac{\Delta B_0}{B_0} = 10^{-4}$ in a cylindrical volume of 1.7 mm diameter and 1.3 mm length (Fig. 2).

The on-board NMR probe is homebuilt and consists of non-magnetic and multi-turn tuning and matching trim capacitors (Voltronics Corp., Salisbury, MD, USA) which were employed to attain resonance at 21.25 MHz. Additionally, the probehead consists of a 12 turns solenoidal micro-coil on a high-resolution glass capillary with1.7 mm outer diameter (OD) and 1.3 mm inner diameter (ID). The solenoidal coil is made of copper wire of diameter 80 μm, has a length of 1 mm and an ID of 1.7 mm. The solenoidal

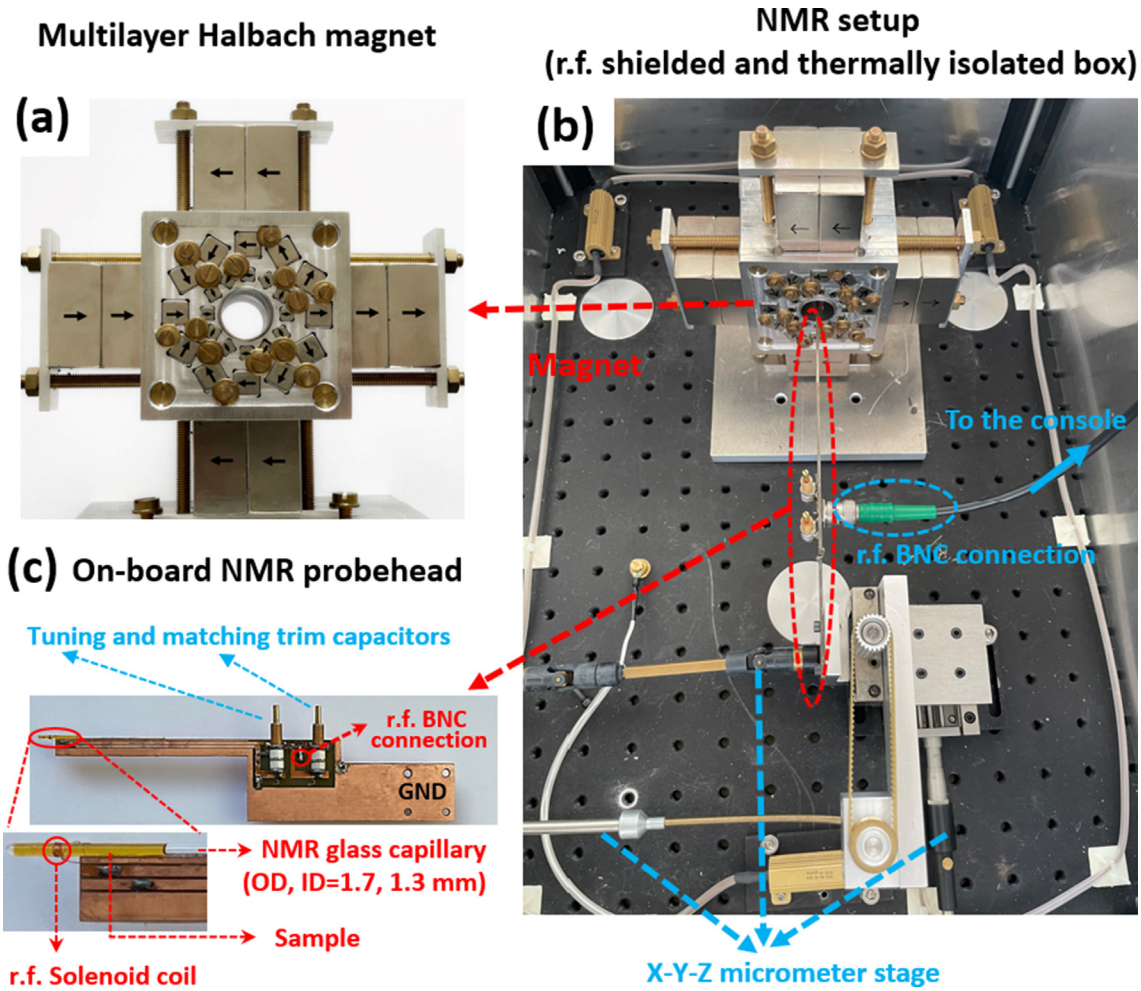

Fig. 2. **(a)** Multilayer Halbach permanent magnet. **(b)** NMR setup (r.f. shielded thermally isolated box). **(c)** The on-board NMR probehead consisting of tuning and matching trim capacitors, r.f. BNC connection, r.f. solenoid coil, NMR glass capillary (OD = 1.7 mm, ID = 1.3 mm) and ground coupling (GND).

coil has an inductance of 3.6 μH. The probehead elements were installed on a printed circuit board of glass-reinforced epoxy laminate (RT4) with a double copper layer of 35 μm thickness [21]. The resonance circuit outline and r.f. BNC copper tracks were obtained on the NMR probehead board using UV lithography. The sweet spot of the magnet was determined by connecting the NMR probe to a homebuilt 3D micrometer stage, while another homebuilt micrometer stage was used to rotate the entire magnet to improve the homogeneity. r.f. shielding and fixed temperature were achieved by placing the NMR setup in a homebuilt metallic box of aluminum (2 mm wall thickness). The box was thermally isolated using a formfitting polyurethane foam jacket and supported with a heating system. The temperature was controlled via a programmable standalone commercial temperature controller. Mechanical vibrations >0.6 Hz were suppressed by using an active vibration isolation system (Halcyonics GmbH, Göttingen, Germany), while the ultra-low vibrations were suppressed by using a passive vibration isolated table. The portable NMR setup is shown in Fig. 2.

All optimal control pulses were obtained employing the robust Krotov algorithm with a SFI of 20 Hz and a RFI of 20 percent, as described in Section 2. The optimal control pulses had a duration of 11 ms for (600.13 MHz) or 50 ms for (21.25 MHz) and typically 2000 iterations of the algorithm were used to obtain convergence, resulting in calculation times of 20 min for an INTEL Core i7 system with 16 GB RAM.

Pulses were calculated in MATLAB, version R2019a. The algorithm used is based on code from literature in reference [18] and was further developed to include robust pulse calculation, i.e., to cope with effects of B_1- and B_0- inhomogeneity. The effect of B_1-inhomogeneity on the performance of the OC pulse is discussed in details in Section 4.1.

The high resolution ^{1}H NMR spectra were measured at a 600 MHz (B_0 = 14.1 T) Bruker AVANCE III spectrometer with a Bruker ASCEND 600 magnet. The probehead employed was a Bruker PABBO room temperature probe with a broadband channel tunable from ^{15}N to ^{31}P. High resolution 5 mm borosilicate glass NMR tubes (Boro600-4–8, Deutero GmbH, Kastellaun, Germany) were used for measurements at 600 MHz. Data acquisition and processing as well as data analysis were conducted with the TopSpin 3.2 software package [22].

4. Results

4.1. Spin editing

The proton NMR hard pulse spectrum of neat cyclopentenone taken at 600.13 MHz is shown in Fig. 3b. In the high-resolution NMR spectrum at 600.13 MHz, the multiplets are well resolved, see Fig. 3a. The same sample was measured with the home-built low-field NMR at 21.25 MHz (Fig. 3c). The signals at −1464.85 Hz and −1232.25 Hz at 600.13 MHz appeared as one signal at 21.25 MHz due to the low resolution: The line width of the low frequency NMR signal was around 16 Hz. To prove, that this

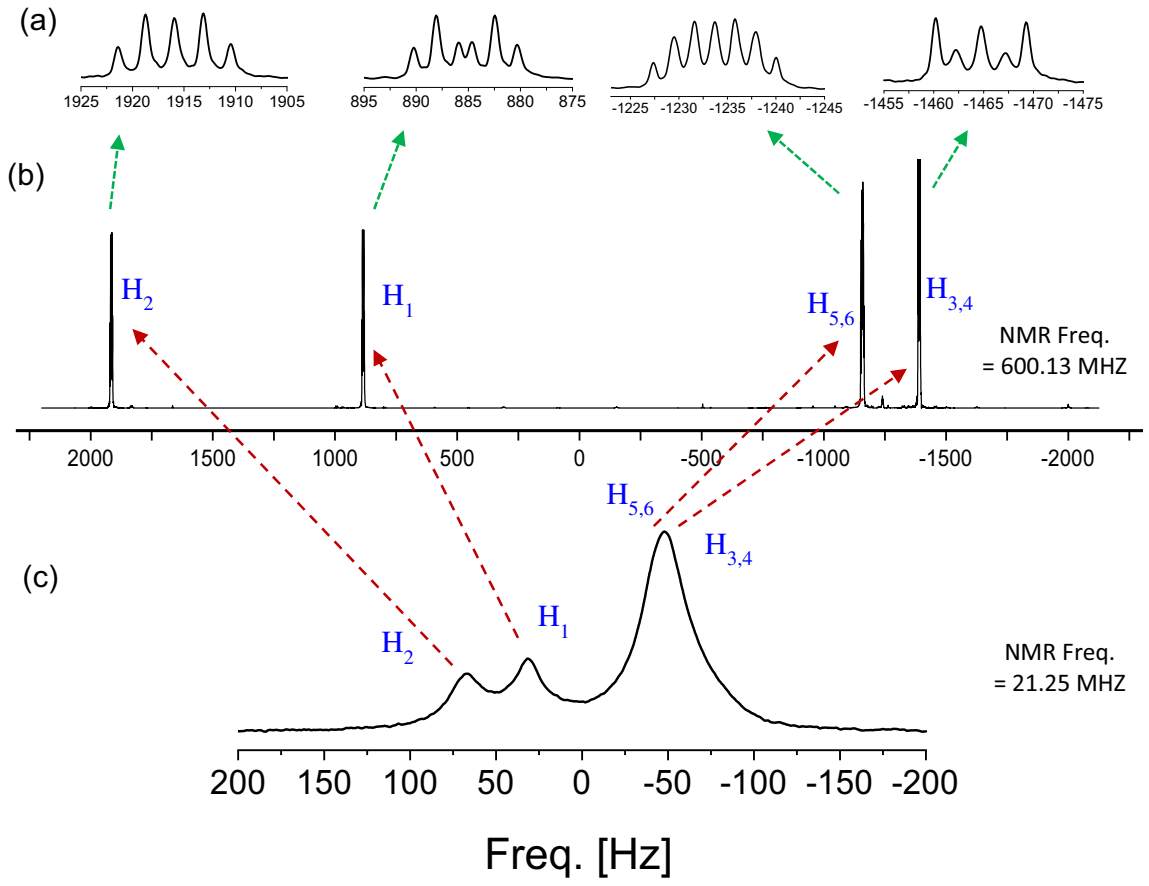

Fig. 3. **(a)** Signal expansions of the NMR hard pulse spectra of cyclopentenone at 600.13 MHz **(b)** The full spectrum at 600.13 MHz **(c)** Spectrum at 21.25 MHz measured using the home-built portable NMR spectrometer.

linewidth is mainly due to field inhomogeneity, an NMR spectrum of acetic acid NMR has been obtained at 21.25 MHz (data not shown), employing the same experimental conditions that were used for the cyclopentenone measurements. The linewidth of the methyl-group signal of acetic acid was found to be 15 Hz. The homogeneous linewidth contribution, as calculated from T_2, was around 2.5 Hz, indicating that the contribution of the magnetic field inhomogeneity is around 12.5 Hz.

The resonance frequencies as well as the coupling constants for both NMR frequencies are given in Fig. 4. The resonance frequencies at 21.25 MHz were obtained both from the experimental spectrum and validated by comparing with the resonance frequencies obtained by downscaling from 600.13 MHz to 21.25 MHz.

The hard pulse spectrum of cyclopentenone is shown in Fig. 3a, with the frequency scale set to 0 Hz in the center of the spectrum. Every stack plot of an optimal control pulse spectrum consists of two NMR spectra; the upper spectrum is the simulated one while the lower spectrum is the experimental one. The experimental spin–spin relaxation time (T_2) values for cyclopentenone (650 and 430 ms at 600.13 MHz and 21.25 MHz, resp.) have been used in the simulations.

Four optimal control pulses were generated by employing the Krotov algorithm at 21.25 MHz to excite protons in the cyclopentenone sequentially during a series of experiments as indicated in Fig. 5 (b-e).

The optimal control pulse for the excitation of the coupled selected protons were calculated in a non-robust way (SFI = RFI = 0) with two control amplitudes corresponding to both phase and amplitude modulation.

The system Hamiltonian of the cyclopentenone spin system is given by:

$$H_{cyc} = 2\pi \sum_{i=1}^{6} \nu_i^{cyc} I_{zH_i}^{cyc} + 2\pi \sum_{i=1}^{6} \sum_{K=i+1}^{6} J_{ik}^{cyc} \hat{\mathbf{I}}_{H_i}^{cyc} \cdot \hat{\mathbf{I}}_{H_k}^{cyc}$$

$$J_{13}^{cyc} = J_{14}^{cyc} = J_{56}^{cyc} = 0, \hat{\mathbf{I}} = I_x, I_y, I_z \tag{6}$$

where $(H_i, i = 1..6)$ denote the ^{1}H spins. The corresponding resonance frequencies $(\nu_i^{cyc}, i = 1..6)$ of cyclopentenone are indicated in Fig. 4. The spin matrices are denoted $\hat{\mathbf{I}}_{H_i}^{cyc}$ with $i = 1..6$and $\hat{\mathbf{I}} = (I_x, I_y, I_z)$.

The calculation was run as a state-to-state transfer with the initial and target operators for all spins chosen as follows:

The initial operator is given as follows

$$I_{ini}^{cyc} = \sum_{i=1}^{6} I_{z_{H_i}}^{cyc} \tag{7}$$

Target operators (TO_0^{cyc}, TO_1^{cyc}, TO_2^{cyc}, TO_3^{cyc} and TO_4^{cyc}) to generate optimal control pulses (0, 1, 2, 3 and 4) to excite proton group0 ($H_1, H_2, H_3, H_4, H_5 and H_6$ in Fig. 5a, hard pulse), group1 ($H_3, H_4, H_5 and H_6$ in Fig. 5b), group 2 ($H_1 and H_2$in Fig. 5c), group3 ($H_1, H_3, H_4, H_5 and H_6$ in Fig. 5d) and group 4 ($H_2, H_3, H_4, H_5 and H_6$ in Fig. 5e) were chosen as in Eqs. (8)–(12).

By introducing the abbreviations: $I_{z_{H_i}}^{cyc} = Z_i and I_{x_{H_i}}^{cyc} = X_i$, and skipping the sum sign, the target operators can be written as follows.

$$TO_0^{cyc} = X_1X_2X_3X_4X_5X_6 \tag{8}$$

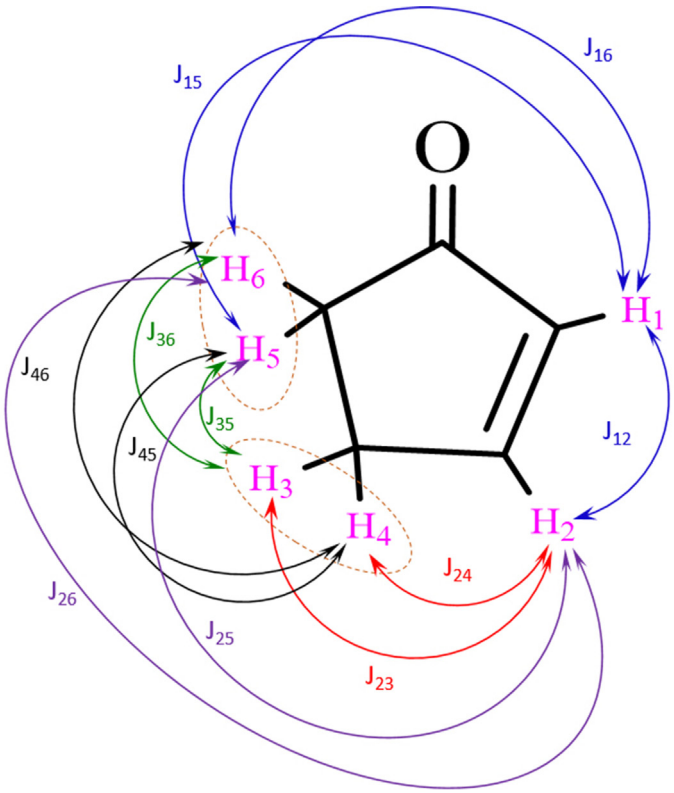

J-coupling [Hz]	Resonance frequencies	
	600.13 MHz	21.25 MHz
J_{12} = 5.65 J_{15} = J_{16} = 2.20 J_{23} = J_{24} = 2.60 J_{25} = J_{26} = 2.30 J_{35} = J_{36} = 2.68 J_{45} = J_{46} = 4.54	ν_1 = 885.26 ν_2 = 1915.89 ν_3 = ν_4 = -1464.85 ν_5 = ν_6 = -1232.25	ν_1 = 31.34 ν_2 = 67.83 ν_3 = ν_4 = -51.86 ν_5 = ν_6 = -43.63

Fig. 4. Visualization of the signal assignments and the coupling network of cyclopentenone. Numerical values are given in the table below.

$$TO_1^{cyc} = Z_1Z_2X_3X_4X_5X_6 \quad (9)$$

$$TO_2^{cyc} = X_1X_2Z_3Z_4Z_5Z_6 \quad (10)$$

$$TO_3^{cyc} = X_1Z_2X_3X_4X_5X_6 \quad (11)$$

$$TO_4^{cyc} = Z_1X_2X_3X_4X_5X_6 \quad (12)$$

The quality factor of the calculation (U denotes the calculated pulse propagator) for e.g., the excitation of the signals of the proton group 1 is given by:

$$\varnothing = real\left(Trace\left(TO_1' U I_{ini}^{cyc} U'\right)\right) \quad (13)$$

The imaginary part is zero within the limits of precision of the calculation.

An excitation factor (EF) has been introduced to quantify the magnitude of the excited (wanted) signal after applying the optimal control pulses with respect to the full excitation using a hard pulse; the ideal excitation factor should be equal to 1. Likewise, a suppression factor (SF) serves to quantify the magnitude of the suppressed (unwanted) signal with respect to the same signal that is excited with a hard pulse; the ideal suppression factor should be equal to zero. EF and SF are included in the plots (Fig. 5) providing direct information about the quality of the optimal control pulses in excitation of the wanted signal and in suppression of the unwanted signal for experimental data.

Fig. 6 shows the amplitude and the phase of the calculated OC pulse for the excitation of the ($H_1, H_3, H_4, H_5 and H_6$) proton groups in cyclopentenone. Remarkably, there is a 2*pi jump of the phase at times below 2.5 ms. A smoothing procedure [18] was introduced to deal with this jump in phase by using an FT of the control amplitude vectors, setting the high frequency components to zero and then performing an inverse FT to return to the control amplitudes. We found that the performance of these smoothed pulses is much poorer than the performance of their unsmoothed counterparts. For this reason, we decided to use unsmoothed pulses throughout this investigation. (SEE Fig. 7.)

The magnitude variation of the targeted signal as a function of the power of the excitation pulse was measured to characterize the effect of B_1- inhomogeneity on the performance of the pulse. The chart (Fig. 8 (a-c)) shows the performance of an OC pulse for cyclopentenone that is acting on group2 spins which is to suppress the signals of (H_3, H_4, H_5 and H_6) and to excite the signals of (H_1 and H_2) as a function of the OC pulse power.

The targeted signal can still be excited with 90% of its nominal amplitude at power levels that are 10% lower or higher than the

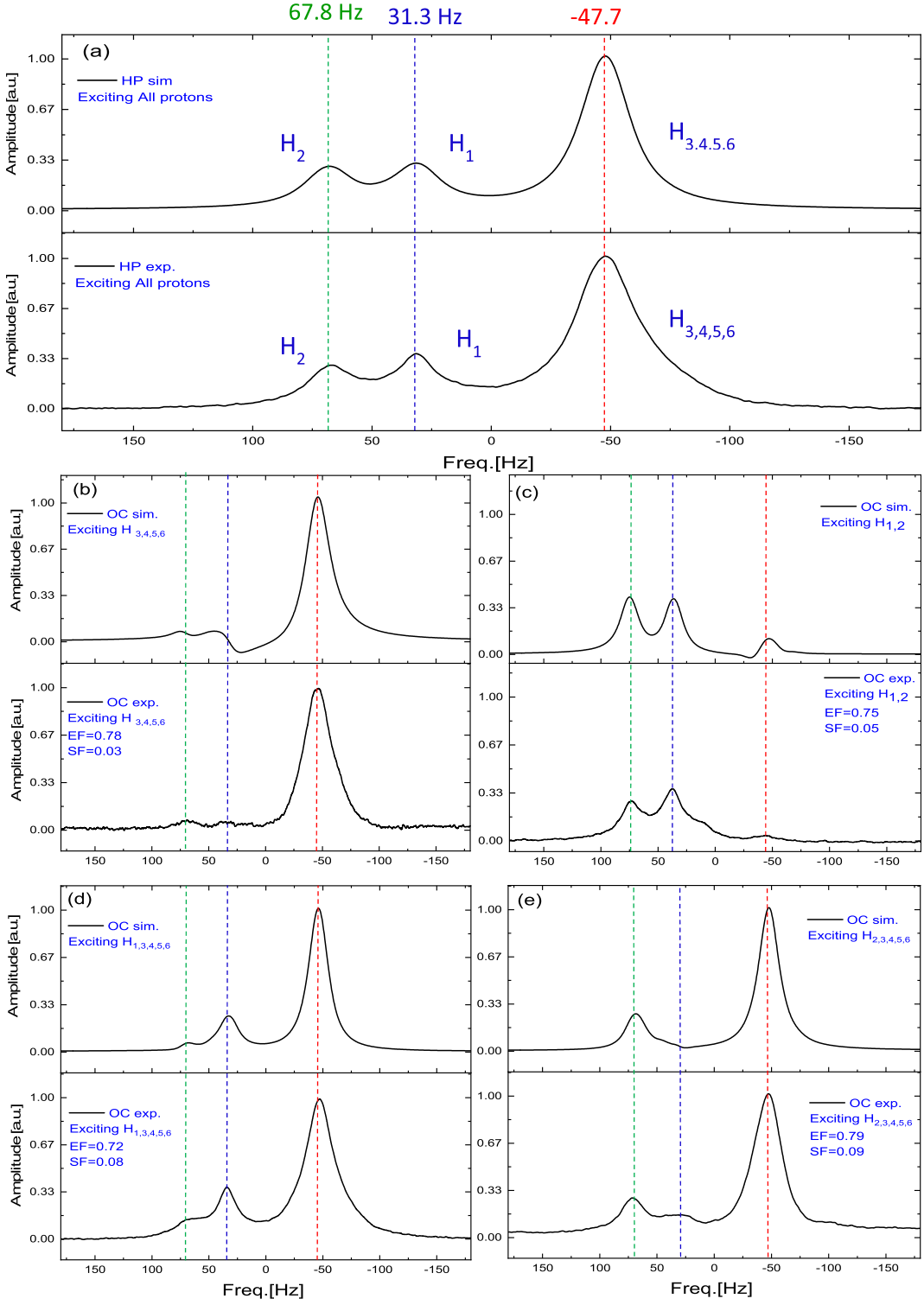

Fig. 5. Simulated (upper spectrum of every stack plot) and experimental (lower spectrum of every stack plot) ^{1}H NMR spectra (21.25 MHz) of cyclopentenone generated by **(a)** a hard pulse and the simulated and the experimental spectra using optimal control pulses to excite **(b)** group1 (H_3, H_4, H_5 and H_6), **(c)** group 2 ($H_1$and H_2), **(d)** group3 ($H_1, H_3, H_4, H_5$and H_6) and **(e)** group 4 (H_2, H_3, H_4, H_5 and H_6).

optimum power level. The suppression of unwanted signal, on the other hand, fails completely at power levels 10% higher or lower than the nominal one. Additionally, OC pulses worked just on resonance, i.e., even slight deviations of the transmitter offset from the resonance condition led to a complete failure of the pulse. The optimized OC power levels for the group1, group2, group3 and group 4 are 0.316, 3.981, 0.502 and 0.199 mW resp.. Additionally, the OC pulses were functioned reasonably at resonance ($O_1 = 0$Hz, B_0 =0.4991328 T, corresponding to NMR frequency of 21.2518194 MHz).

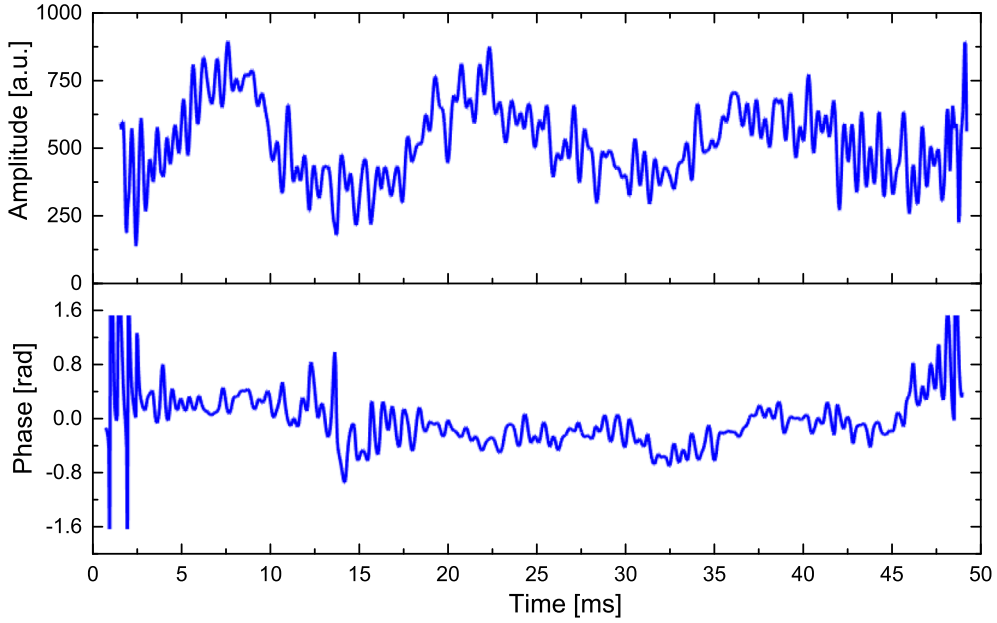

Fig. 6. Pulse shape (amplitude (top) and phase (down)) of a cyclopentenone OC pulse for (H_1, H_3, H_4, H_5andH_6)excitation.

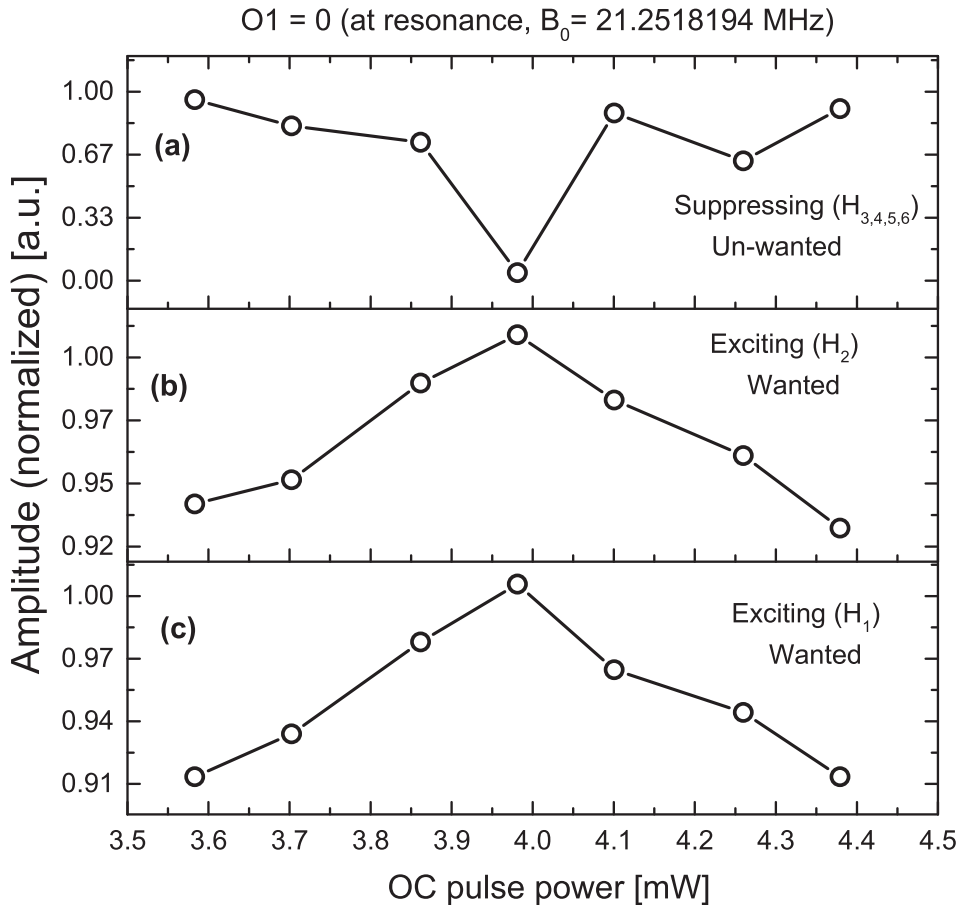

Fig. 7. Performance of an OC pulse for cyclopentenone that is to suppress the signals of (H_3, H_4, H_5 and H_6) and to excite the signals of (H_1 and H_2) as a function of the OC pulse power. The chart shows the effect of B_1-inhomogeneity on the performance of the pulse.

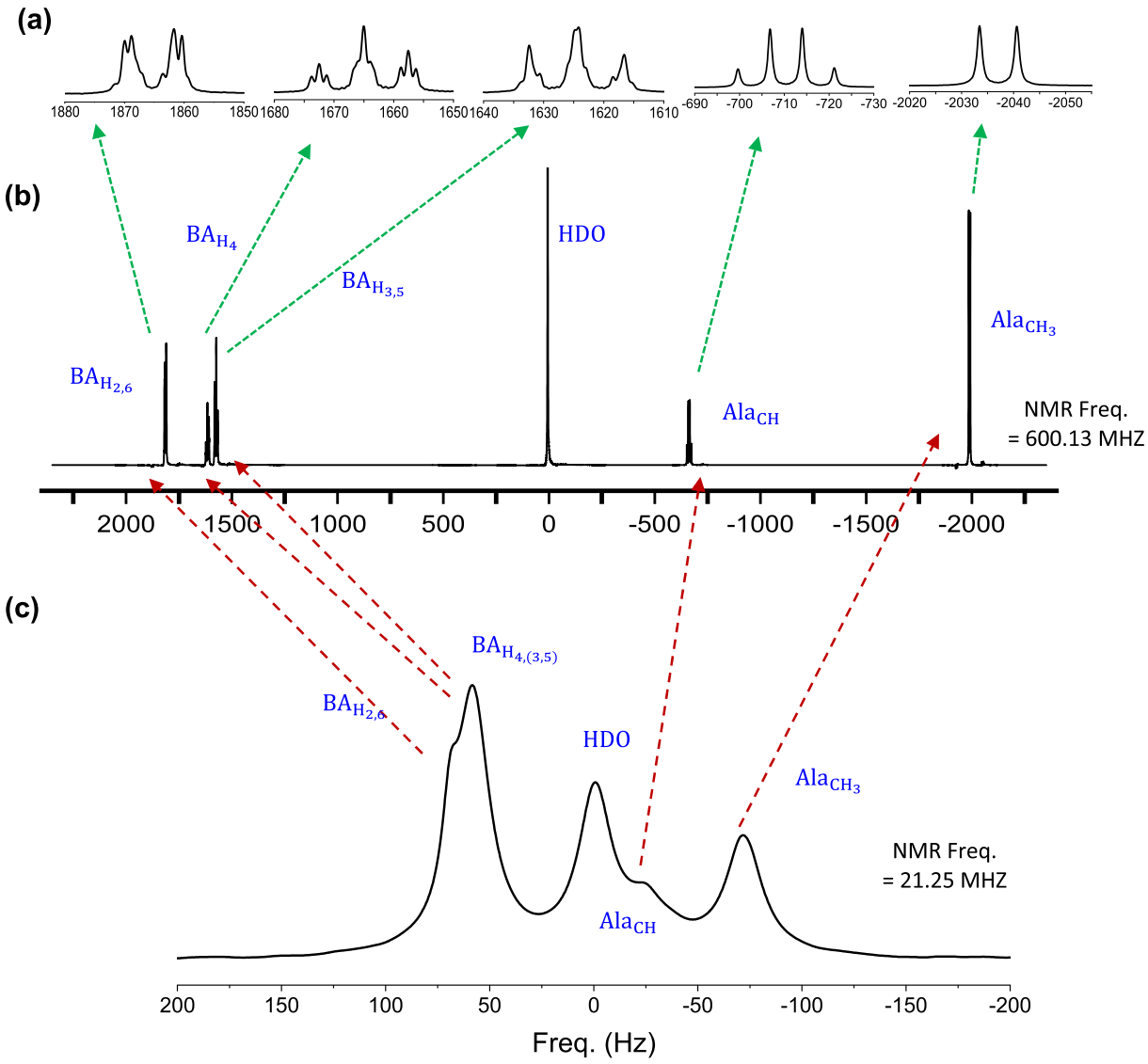

Fig. 8. **(a)** The enlargements of the signals of the 600.13 MHz NMR spectrum showing the splitting patterns. **(b)** 600.13 MHz NMR spectrum (full spectrum). **(c)** The proton NMR hard pulse spectrum of a BA and Ala mixture measured at 21.25 MHz with the home-built low frequency NMR spectrometer.

4.2. Editing of full spin systems in a multisystem mixture

An equimolar benzoic acid (BA) and alanine (Ala) mixture was used for demonstrating subspectral editing (of either BA or Ala signals) using OC pulses.

The proton NMR hard pulse spectra of the BA/Ala mixture taken at 21.25 MHz and 600.13 MHz and the enlargements of the resolved multiples at 600.13 MHz are shown in Fig. 8a, 8b and 8c, resp..

The three multiplet signals of the BA spectrum appeared as one broad signal with a shoulder at 21.25 MHz because their chemical shift differences are smaller than the linewidth (while they are well resolved at 600.13 MHz). The two Ala spectral lines appeared as two separate signals, the Ala CH-signal appearing at –22.5 Hz showed, however, a partial superposition with the water signal.

Similar to the analysis of cyclopentenone, the chemical shifts and the coupling constants of BA and Ala were determined from a first order analysis (Fig. 9) of the spectrum at 600.13 MHz. Afterwards, the resonance frequencies at 21.25 MHz were obtained by downscaling the resonance frequencies to 21.25 MHz.

Optimal control pulses were calculated to excite either BA or Ala as a spectral editing experiment. In order to speed up the calculations, a system approach was applied, i.e., two systems corresponding to the two compounds were chosen. The strong coupling Hamiltonian of the system 1 (BA) is given by

$$H_{cyc} = 2\pi \sum_{i=2}^{6} \nu_i^1 I_{zH_i}^1 + 2\pi \sum_{i=2}^{6} \sum_{K=i+1}^{6} \mathrm{J}_{ik}^1 \hat{\mathbf{I}}_{H_i}^1 \cdot \hat{\mathbf{I}}_{H_k}^1$$

$$\mathrm{J}_{25}^1 = \mathrm{J}_{26}^1 = \mathrm{J}_{35}^1 = \mathrm{J}_{36}^1 = 0, \hat{\mathbf{I}} = I_x, I_y, I_z \tag{14}$$

where $(H_i, i = 2..6)$ denote the spins, and the corresponding resonance frequencies $(\nu_i^1, i = 2..6)$ of BA and are indicated in Fig. 9. The corresponding spin matrices are denoted $\hat{\mathbf{I}}_{H_i}^1$ with $i = 2..6$and $(\hat{\mathbf{I}} = I_x, I_y, I_z)$.

The Hamiltonian of system 2 (Ala) is given by:

$$H_{Ala}^2 = 2\pi \sum_{i=2}^{4} \nu_i^2 I_{zH_i}^2 + 2\pi \sum_{i=1}^{3} \mathrm{J}_{1i}^2 \hat{\mathbf{I}}_{H_1}^2 \hat{\mathrm{A}} \cdot \hat{\mathbf{I}}_{H_{i+1}}^2, \left(\hat{\mathbf{I}} = I_x, I_y, I_z\right) \tag{15}$$

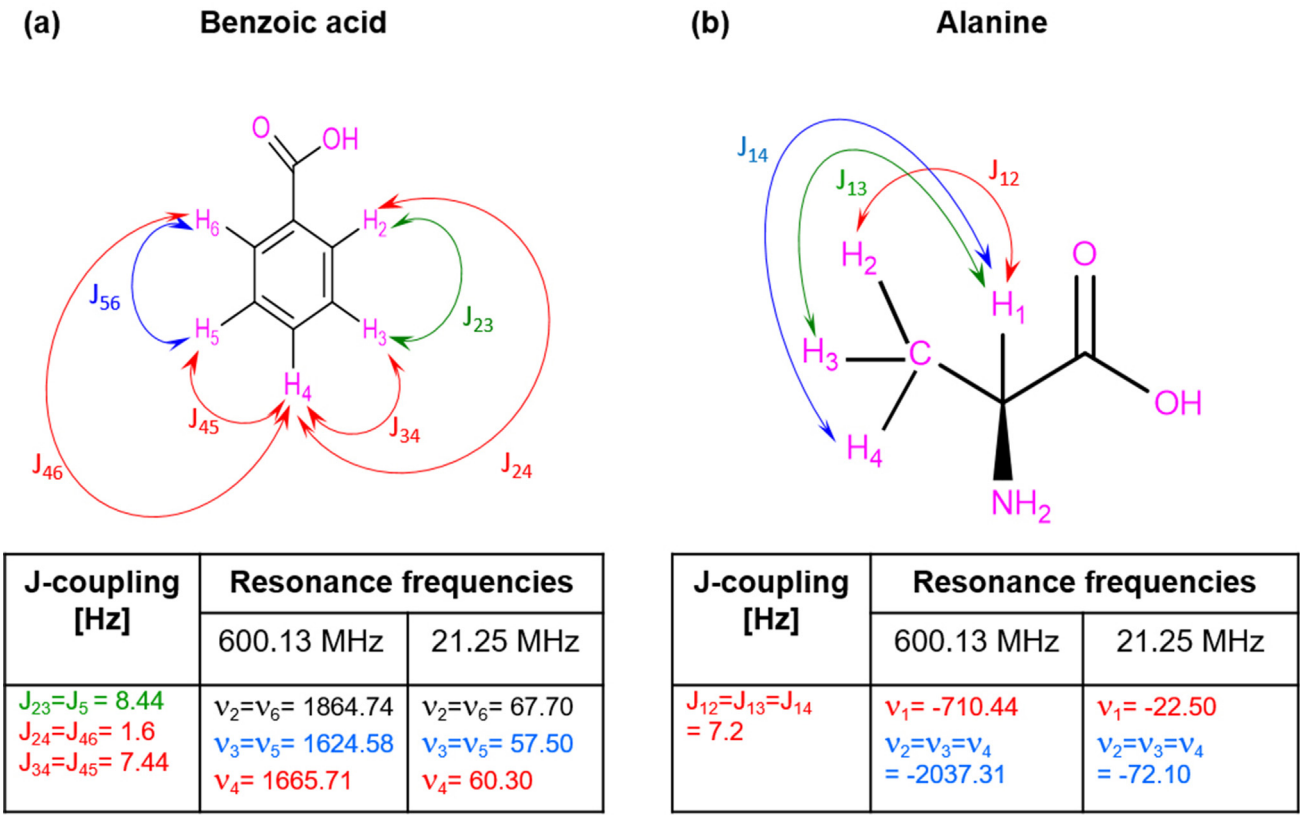

J-coupling [Hz]	Resonance frequencies	
	600.13 MHz	21.25 MHz
$J_{23}=J_5$ = 8.44 $J_{24}=J_{46}$= 1.6 $J_{34}=J_{45}$= 7.44	$\nu_2=\nu_6$= 1864.74 $\nu_3=\nu_5$= 1624.58 ν_4= 1665.71	$\nu_2=\nu_6$= 67.70 $\nu_3=\nu_5$= 57.50 ν_4= 60.30

J-coupling [Hz]	Resonance frequencies	
	600.13 MHz	21.25 MHz
$J_{12}=J_{13}=J_{14}$ = 7.2	ν_1= -710.44 $\nu_2=\nu_3=\nu_4$ = -2037.31	ν_1= -22.50 $\nu_2=\nu_3=\nu_4$ = -72.10

Fig. 9. Visualization of the resonance frequencies and the coupling network of (a) Benzoic acid and (b) Alanine.

where $(H_i, i = 1..4)$ denote the spins of Ala and are indicated in Fig. 9. The corresponding spin operators are denoted $\hat{\mathbf{I}}^2_{H_i}$ with $i = 1..4$and $(\hat{\mathbf{I}} = I_x, I_y, I_z)$. The resonance frequencies $(v_i^2,\ i = 1..4)$ are indicated as well in Fig. 9 for both NMR frequencies.

The calculation was run as a state-to-state transfer with the initial operators for both systems being as follows:

$$I^1_{ini_{BA}} = \sum_{i=2}^{6} I^1_{zH_i}(Initialoperator1) \tag{16}$$

$$I^2_{ini_{Ala}} = \sum_{i=1}^{4} I^2_{zH_i}(Initialoperator2) \tag{17}$$

Target operators (TO_1, TO_2) to generate optimal control pulses to excite spin system 1 (BA) and spin system 2 (Ala) (Fig. 10a) are denoted as follows:

$$TO_1 = \sum_{i=2}^{6} I^1_{xH_i}(Targetoperator1) \tag{18}$$

$$TO_2 = \sum_{i=1}^{4} I^2_{xH_i}(Targetoperator2) \tag{19}$$

And to excite system 1 (Ba) (Fig. 10b):

$$TO_1 = \sum_{i=2}^{6} I^1_{xH_i}(Targetoperator1) \tag{20}$$

$$TO_2 = \sum_{i=1}^{4} I^2_{zH_i}(Targetoperator2) \tag{21}$$

And to excite system 2 (Ala) (Fig. 10c):

$$TO_1 = \sum_{i=2}^{6} I^1_{zH_i}(Targetoperator1) \tag{22}$$

$$TO_2 = \sum_{i=1}^{4} I^2_{xH_i}(Targetoperator2) \tag{23}$$

The quality factor of the calculation (U_1 and U_2 denote the calculated pulse propagators for system 1 and system 2, resp.) is given by:

$$\varnothing = real\left(Trace\left(TO_1' U_1 I^1_{ini} U_1'\right)\right) + real\left(Trace\left(TO_2' U_2 I^1_{ini} U_2'\right)\right) \tag{24}$$

The imaginary part is zero within the limits of precision of the calculations.

Three optimal control pulses were calculated, simulated and performed at 21.25 MHz.

The simulated and measured ^{1}H NMR spectra using the first optimal control pulse at 21.25 MHz to excite both systems (Ba and Ala) as a hard pulse (HP) are shown in Fig. 10a. The second optimal control pulse was calculated to excite the BA proton spectrum and to suppress the Ala proton spectrum, while the third optimal control pulse was calculated to perform in reverse order. The obtained simulated and experimental spectra are shown in Fig. 10b and 10c, respectively.

5. Discussion and conclusions

To show the performance and the advantages of optimal control pulses over a selective excitation based on Gaussian pulses, the cyclopentenone experiments that were done with OC pulses were also attempted with Gaussian pulses. The applied Gaussian pulse had a 1% cutoff, offset at the targeted signal, a maximum power level of 3.16 μW and a pulse length of 21.2 ms. The excitation and suppression factors found for both cases are given in Table 1. The Gaussian pulse suppresses the unwanted signal by a factor of SF = 0.03 which is comparable to the performance of a Krotov selective pulse. However, the EF values of the targeted signals

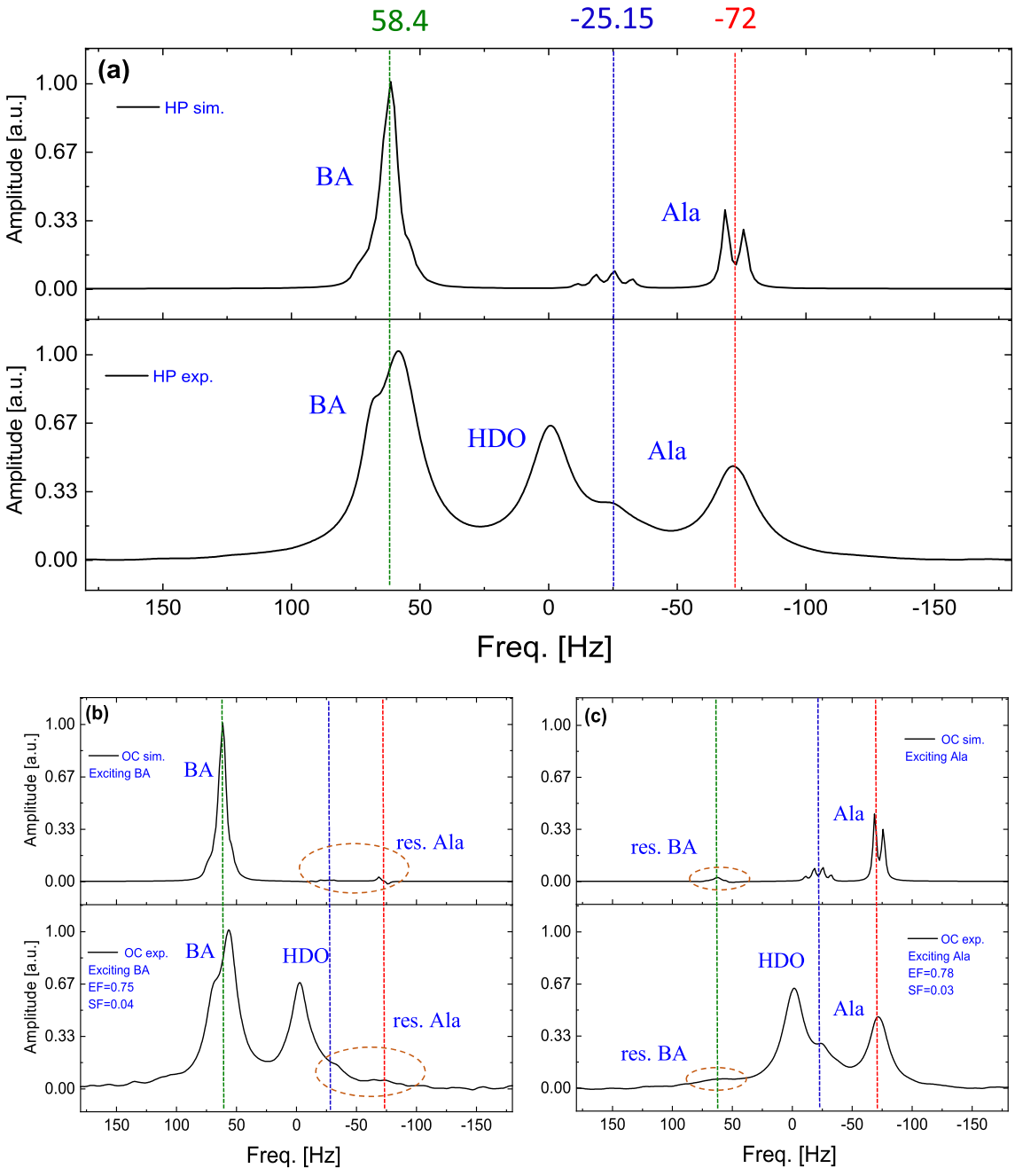

Fig. 10. Simulated (upper spectrum of every stack plot) and experimental (lower spectrum of every stack plot) ^{1}H NMR spectra (21.25 MHz) of BA and Ala mixture generated by optimal control pulse to excite **(a)** both systems (Ba and Ala) as a hard pulse (HP), **(b)** spin system 1 (BA) and **(c)** spin system 2 (Ala). Signal of HDO appeared in the experimental spectra but not in the simulation.

using a Gaussian pulse (0.5 on average) show significant differences compared to those measured with OC pulses (0.77 on average). Moreover, the results obtained for group 2 to group 4 reveal that Gaussian pulses can only be applied on a continuous range of frequencies: This is, however, usually not the case for metabolites, which have their signals spread over a wide range of frequencies, with signal ranges of other metabolites in between. Hence, Gaussian pulses are inappropriate for targeted metabolic profiling using NMR.

To conclude, we have shown, that optimal control pulses can be applied for subspectral editing at a field strength as low as 0.5 T, i.e., under conditions of strong coupling. Employing the Krotov algorithm to a mixture of benzoic acid and alanine, compound selective excitation pulses could be calculated. These pulses excite either the signal of benzoic acid or that of alanine with very little crosstalk, namely 5% from alanine and 4% from benzoic acid, resp.. Even for the spin system of cyclopentenone, where the aliphatic and olefinic protons are coupled to each other, the signals of four groups of protons mostly arising from both aliphatic and olefinic protons could be edited with a crosstalk of unwanted signal in the low percent range. In this way, selective excitation pulses for individual components in multi component mixtures become available. This resembles the concept of a programmable detector, which excites and detects just one target compound at a time thus circumventing the problem of signal superposition. Combined with a magnet that has a large homogeneous volume like a Halbach magnet [22], the aforementioned approach would open low field NMR for new applications such as targeted metabolomics. When

Table 1
The EF and SF factors of the signal groups excited using Gaussian and OC (Krotov) pulses. EF and SF Factors calculated using the absolute integration of the wanted and unwanted signal, resp. with respect to the absolute integration of the same signals after excitation with a hard pulse.

(a)

Cyclopentenone

Factor	**Group 1** $H_3, H_4, H_5 and H_6$		**Group 2** $H_1 and H_2$		**Group 3** $H_1, H_3, H_4, H_5 and H_6$		**Group 4** $H_2, H_3, H_4, H_5 and H_6$	
	OC Krotov	**Gaussian**	**OC Krotov**	**Gaussian**	**OC Krotov**	**Gaussian**	**OCKrotov**	**Gaussian**
EF	0.80	0.52	0.76	n.p.	0.74	n.p.	0.78	n.p.
SF	0.03	0.03	0.06	n.p.	0.05	n.p.	0.03	n.p.

(b)

Factor	**Benzoic acid**		**Alanine**	
	OC (Krotov)	Gaussian	OC (Krotov)	Gaussian
EF	0.78	0.55	0.77	0.53
SF	0.05	0.02	0.04	0.03

n.p.: not possible (because the signals fall in a frequency range where other wanted signal are showing up and then the unwanted signals cannot be suppressed selectively (continuous frequency range can be excited or suppressed)).

equipped with a library of spectral editing pulses, a cheap and low footprint NMR spectrometer could be applied in point of care settings like doctors' offices or intensive care units and increase the throughput of clinical [23] samples.

Declaration of Competing Interest

The authors declare that they have no known competing financial interests or personal relationships that could have appeared to influence the work reported in this paper.

Acknowledgment

Financial support by the Ministerium für Innovation, Wissenschaft und Forschung des Landes Nordrhein-Westfalen, the Senatsverwaltung für Wirtschaft, Technologie und Forschung des Landes Berlin, and the Bundesministerium für Bildung und Forschung is gratefully acknowledged.

Appendix

App 1: Krotov algorithm

The functional J, given by

$$J = \varnothing - \lambda \int_0^T \sum_k \omega_k^2(t) dt \tag{A1}$$

has to be optimized under the constraint of the Liouville equation,

$$\frac{dU(t)}{dt} = -iH(t)U(t) \tag{A2}$$

with the Hamiltonian

$$H(t) = H^{\circ} + \sum_k \omega_k I_k, \tag{A3}$$

where H_0 and $\sum_k \omega_k I_k$ denote the system Hamiltonian and the control Hamiltonian, respectively, resulting in

$$\frac{d}{dt}U_n(t) = -i\left[H_{\circ} + \sum_k \omega_{k,n} I_k\right] U_n(t) \tag{A4}$$

where n denotes the number of the iteration. The Liouville Eq. (A4) is introduced to (A1) as a constraint using a complex valued operator, called back propagation operator (B) as a Lagrange multiplier. As J has to remain real valued, the complex conjugate of the Lagrange multiplier term has to be added as well:

$$J = \varnothing - \lambda \int_0^T \sum_k \omega_k^2(t) dt \tag{A5}$$

$$- \int_0^T Tr\left\{ B^+(t)\left[\frac{d}{dt}U(t) + iH(t)U(t)\right]\right\} dt$$

$$- \int_0^T Tr\left\{ \left[\frac{d}{dt}U^+(t) - iU^+(t)H(t)\right] B(t)\right\} dt$$

where U^+ and B^+ denote the adjoint operators of U and B, resp.. The optimization requires the derivatives of the functional J with respect to the control parameters to be zero at a stationary point, resulting in the three equations

$$\frac{d}{dt}B(t) = -iH(t)B(t) \tag{A6}$$

$$B(t) = \frac{\partial \varnothing_i}{\partial U(T)} \tag{A7}$$

$$\omega_k(t) = \frac{1}{\lambda} ImTr\left\{ \left[B^+(t) I_k U(t)\right]\right\} \tag{A8}$$

As the functional J has to increase with each iteration n, the following expression must be positive,

$$\varnothing_{n+1} - \phi_n - \lambda \sum_k \int_0^T \left[\omega_{k,n+1}^2(t) - \omega_{k,n}^2(t)\right] dt \tag{A9}$$

Importing the stationary point conditions and evolving the propagators using the second order Strang method [16], one arrives at

$$f_j\left(\omega_j^{'}\right) = 2Re\left[Tr\left\{ \left(\exp\left(i\Delta t \sum_k \omega_{kj-1} H_k \right) \times \exp\left(-i\Delta t \sum_k \omega_{kj-1}^{'} H_k \right) - E \right) A U_{j-1}^{'} B_{j-1} A^+ \right\} \right] - \Delta t \lambda \sum_k \left(\omega_{kj-1}^{'} - \omega_{kj-1}\right)\left(\omega_{kj-1}^{'} + \omega_{kj-1}\right) \tag{A10}$$

which has to be maximized in order to keep the functional difference positive. Here the primed and unprimed variables refer to iteration number $n+1$ and n, respectively, j denotes the number of the time step of length $\Delta t, A = e^{-i0.5\Delta t H_0}$ and E is the identity operator. The minimization of $-f_j\left(\omega_j^{'}\right)$ is started with an appropriate initial guess for the ω_j, using a quasi-Newton optimizer.

References

[1] B. Blümich, Low-field and benchtop NMR, J. Magn. Reson. 306 (2019) 27.
[2] P. Blümler, F. Casanova, Hardware developments: Halbach magnet arrays, 2016, Nan Sun and Donhee Ham, 158-182,10.1039/9781782628095-00133.
[3] J. Anders, K. Lips, MR to go, J. Magn. Reson. 306 (2019) 118.
[4] M. Grootveld, B. Percival, M. Gibson, Y. Osman, M. Edgar, M. Molinari, M.L. Mather, Progress in low-field benchtop NMR spectroscopy in chemical and biochemical analysis, Anal. Chim. Acta 1067 (2019) 11.
[5] B. Luy, Towards portable high-resolution NMR spectroscopy, Angew. Chem. Int.l Ed. 50 (2011) 354.
[6] L.H. Antonides, R.M. Brignall, A. Costello, J. Ellison, S.E. Firth, N. Gilbert, B.J. Groom, S.J. Hudson, M.C. Hulme, J. Marron, Z.A. Pullen, T.B.R. Robertson, C.J. Schofield, D.C. Williamson, E. Kate Kemsley, O.B. Sutcliffe, R.E. Mewis, Rapid identification of novel psychoactive and other controlled substances using low-field 1H NMR spectroscopy, ACS Omega 4 (2019) 7103.
[7] G. Assemat, B. Gouilleux, D. Bouillaud, J. Farjon, V. Gilard, P. Giraudeau, M. Malet-Martino, Diffusion-ordered spectroscopy on a benchtop spectrometer for drug analysis, J. Pharm. Biomed. Anal. 160 (2018) 268.
[8] J. Duffy, A. Urbas, M. Niemitz, K. Lippa, I. Marginean, Differentiation of fentanyl analogues by low-field NMR spectroscopy, Anal. Chim. Acta 1049 (2019) 161.
[9] D. Fallaise, H.B. Tweedie, J. Konzuk, C. Cheyne, E.E. Mack, J.G. Longstaffe, Practical application of H-1 benchtop NMR spectroscopy for the characterization of a nonaqueous phase liquid from a contaminated environment, Magn. Reson. Chem. 57 (2019) 93.
[10] M. Leutzsch, A.J. Sederman, L.F. Gladden, M.D. Mantle, In situ reaction monitoring in heterogeneous catalysts by a benchtop NMR spectrometer, Magn. Reson. Imag. 56 (2019) 138.
[11] D. Golowicz, K. Kazimierczuk, M. Urbanczyk, T. Ratajczyk, Monitoring hydrogenation reactions using benchtop 2D NMR with extraordinary sensitivity and spectral resolution, Chemistryopen 8 (2019) 196.
[12] B. Gouilleux, N.V. Christensen, K.G. Malmos, T. Vosegaard, Analytical evaluation of low-field P-31 NMR spectroscopy for lipid analysis, Anal. Chem. 91 (2019) 3035.
[13] M.K. Sorensen, N.M. Balsgart, O. Jensen, N.C. Nielsen, T. Vosegaard, Fast wide-line solid-state NMR on a low-cost benchtop spectrometer, ChemPhysChem 19 (2018) 2985.
[14] T. Castaing-Cordier, D. Bouillaud, P. Bowyer, O. Gonalves, P. Giraudeau, J. Farjon, Highly resolved pure-shift spectra on a compact NMR spectrometer, ChemPhysChem 20 (2019) 736.
[15] E.R. McCarney, R. Dykstra, P. Galvosas, Evaluation of benchtop NMR Diffusion Ordered Spectroscopy for small molecule mixture analysis, Magn. Reson. Imag. 56 (2019) 103.
[16] Y. Maday, J. Salomon, G. Turinici, Monotonic time-discretized schemes in quantum control, Numer. Mathem. 103 (2006) 323.
[17] I.I. Maximov, Z. Tosner, N.C. Nielsen, Optimal control design of NMR and dynamic nuclear polarization experiments using monotonically convergent algorithms, J. Chem. Phys. 128 (2008) 184505.
[18] I.I. Maximov, J. Salomon, G. Turinici, N.C. Nielsen, A smoothing monotonic convergent optimal control algorithm for nuclear magnetic resonance pulse sequence design, J. Chem. Phys. 132 (2010) 084127.
[19] M. Holbach, J. Lambert, D. Suter, Optimized multiple-quantum filter for robust selective excitation of metabolite signals, J. Magn. Reson. 243 (2014) 8.
[20] M. Holbach, J. Lambert, S. Johst, M.E. Ladd, D. Suter, Optimized selective lactate excitation with a refocused multiple-quantum filter, J. Magn. Reson. 255 (2015) 34.
[21] M. Gupta, C.P. Safvan, K. Singh, D.K. Lobiyal, P. Yadav, S. Singh, Radio frequency planar coil based on-chip probe for portable nuclear magnetic resonance, IEEE Sens. J. 19 (2019) 2500.
[22] H.P. Raich, P. Blümler, Design and construction of a dipolar Halbach array with a homogeneous field from identical bar magnets: NMR Mandhalas. Conc. Magn. Reson. B Magn Reson. Eng. 23 (2004) 16.
[23] G. Assemat, S. Balayssac, A. Gerdova, V. Gilard, C. Caillet, D. Williamson, M. Malet-Martino, Benchtop low-field ^{1}H Nuclear Magnetic Resonance for detecting falsified medicines, Talanta 196 (2019) 163–173.